# Chemical Characteristics and Source of $PM_{2.5}$ in Hohhot, a Semi-arid City in Northern China: Insight from the COVID-19 Lockdown

Haijun Zhou[1,2,3#], Tao Liu[4#], Bing Sun[5], Yongli Tian[4], Xingjun Zhou[4], Feng Hao[4], Xi Chun[1,2,3], Zhiqiang Wan[1,2,3], Peng Liu[1], Jingwen Wang[1], Dagula Du[6]

[1]College of Geographical Sciences, Inner Mongolia Normal University, Hohhot 010022, China
[2]Provincial Key Laboratory of Mongolian Plateau's Climate System, Inner Mongolia Normal University, Hohhot 010022, China
[3]Inner Mongolia Repair Engineering Laboratory of Wetland Eco-environment System, Inner Mongolia Normal University, Hohhot 010022, China
[4]Environmental Monitoring Center Station of Inner Mongolia, Hohhot 010011, China
[5]Hohhot Environmental Monitoring Branch Station of Inner Mongolia, Hohhot 010030, China
[6]Environmental Supervision Technical Support Center of Inner Mongolia, Hohhot 010011, China

*Correspondence to*: Haijun Zhou (hjzhou@imnu.edu.cn)

[#] H. Zhou and T. Liu contributed equally to this work.

**Abstract.** A knowledge gap exists concerning how chemical composition and sources respond to implemented policy control measures for aerosols, particularly in a semi-arid region. To address this, a single year's offline measurement was conducted in Hohhot, a semi-arid city in northern China, to reveal the driving factors of severe air pollution in a semi-arid region and assess the impact of the COVID-19 lockdown measures on chemical characteristics and sources of $PM_{2.5}$. Organic matter, mineral dust, sulfate, and nitrate, accounted for 31.5%, 14.2%, 13.4%, and 12.3% of the total $PM_{2.5}$ mass, respectively. Coal combustion, vehicular emissions, crustal sources, and secondary inorganic aerosols were the main sources of $PM_{2.5}$ in Hohhot, at 38.3%, 35.0%, 13.5%, and 11.4%, respectively. Due to the coupling effect of emission reduction and improved atmospheric conditions, the concentration of secondary inorganic components, organic matter, and elemental carbon decline substantially from the pre-lockdown (pre-LD) period to the lockdown (LD) and post-lockdown (post-LD) periods. The source contribution of secondary inorganic aerosols increased (from 21.1 to 37.8%), whereas the contribution of vehicular emissions was reduced (35.5% to 4.4%) due to lockdown measures. The rapid generation of secondary inorganic components caused by unfavorable meteorological conditions during lockdown led to serious pollution. This study elucidates the complex relationship between air quality and environmental policy.

## 1 Introduction

With the rapid development of industrialization and urbanization, many developing countries, such as China and India, have suffered severe air pollution, especially from fine particulate matter ($PM_{2.5}$, aerodynamic diameter ≤ 2.5 μm). To improve air quality, China has implemented various clean air policies (Zhang et al., 2019). As a result, the annual mean $PM_{2.5}$ concentration in China decreased from 50 μg/m$^3$ in 2015(MEEC, 2015) to 33 μg/m$^3$ in 2020 (MEEC, 2020). However, the mean level of $PM_{2.5}$ is still much higher than the new guideline of the World Health Organization (5μg/m$^3$) (WHO, 2021). It is a challenge to decrease the level of $PM_{2.5}$ to such a low level in China, especially in northern China, which consumes the majority of coal for winter heating. Insufficient understanding of the complex relationship between air quality and environmental policy limits the effectiveness of our control measures to improve air quality.

To limit the spread of the COVID-19 pandemic, most cities around the world implemented strict lockdown measures, and the anthropogenic emission of air pollutants was reduced substantially, which in turn has caused considerable changes in the chemical composition and sources of $PM_{2.5}$. The lockdown provided a good opportunity to study the effect of emission reduction on air quality. In addition, this scenario can be used by policymakers to formulate effective policies to prevent atmospheric pollution. Stringent traffic restrictions during the COVID-19 lockdown led to important reductions in the concentrations of elemental carbon, metals, and nitrate in an urban site of the western Mediterranean (Clemente et al., 2022). The substantial reduction in nitrate in the Beijing-Tianjin-Hebei region during the lockdown period was attributed to the drastic reduction in vehicular movement and the suspension of public transport (Sulaymon et al., 2021). Primary pollutants were reported to have decreased dramatically due to the lockdown measures, while secondary pollutants were reported to have increased (Chang et al., 2020; Huang et al., 2021; Zheng et al., 2020). Secondary pollutants like $PM_{2.5}$ and $O_3$ depend more strongly on weather conditions and show a limited response to emission changes in single sectors (Matthias et al., 2021; Gao et al., 2021).

Extensive studies have been conducted to investigate the responses of atmospheric pollutants to emission reduction during the COVID-19 lockdown measures. However, most of the previous studies are based on online observation and/or satellite-derived data and have focused on the changes in atmospheric pollutants, influence of meteorological conditions, and emission reduction. Relatively few studies have focused on the chemical composition and sources of $PM_{2.5}$ in semi-arid regions, especially using offline measurement. Source apportionment using an online dataset is impeded by the missing information on Si and Al (Gao et al., 2016), resulting in considerable uncertainty in the estimation of dust sources. Mineral dust is considered to be one of the main components of aerosols in semi-arid regions (Kumar and Sarin, 2009; Wang et al., 2016). As a typical semi-arid city of northern China, Hohhot suffers frequent air pollution in spring and winter. The chemical characteristics, sources, and their response to implemented control measures in this region are still unclear.

In response to the substantial reduction in anthropogenic emission, the concentration of $PM_{2.5}$ in most of the European cities (Matthias et al., 2021; Tobías et al., 2020; Collivignarelli et al., 2020;

Gualtieri et al., 2020; Gkatzelis et al., 2021), Latin American cities (Mendez-Espinosa et al., 2020; Nakada and Urban, 2020; Hernández-Paniagua et al., 2021), US cities (Pata, 2020), Indian cities (Sharma et al., 2020), Chinese cities (Bao and Zhang, 2020), and the southeast Asia region (Kanniah et al., 2020) have decreased substantially, compared to pre-LD periods and/or previous years. However, compared with the decreasing trends of most of the cities in the world, the concentrations of $PM_{2.5}$ in some cities of the North China Plain have increased unexpectedly. An increase ($p$<0.01) in $PM_{2.5}$ was found in Hohhot during the LD period, whereas a considerable improvement was reported in most of the cities globally. The response of chemical composition and sources of $PM_{2.5}$ in Hohhot to lockdown measures and the driving factors behind the abnormal increase in $PM_{2.5}$ are still unclear. The anomalously enhanced nitrate in Tianjin during the LD period is a response to the abnormal increase in relative humidity (Ding et al., 2021), The abnormal increase in $PM_{2.5}$ in northern China during the LD period was probably caused by uninterrupted emissions from power plants and petrochemical facilities, as well as the influence of adverse weather conditions (Gao et al., 2021). The extreme reduction in anthropogenic emissions did not address the occurrences of severe haze events in northern China because of unfavorable meteorological events (Le et al., 2020; Shi et al., 2021), increased atmospheric oxidizing capacity (Wang et al., 2020), enhanced secondary formation (Chang et al., 2020; Huang et al., 2021), and regional transport (Shen et al., 2021; Lv et al., 2020; Zhang et al., 2021). There is no consensus on the reasons for the unexpected increase in $PM_{2.5}$ during the LD period. It is therefore essential to conduct a comprehensive study on the chemical composition and sources of $PM_{2.5}$ in this region, especially during the LD period.

The main objectives of this study were to (1) identify the chemical characteristics and sources of $PM_{2.5}$ in a semi-arid city, (2) investigate the impact of COVID-19 lockdown measures on the chemical composition and sources, (3) reveal the causes of the rapid increase in $PM_{2.5}$ during different heavy pollution episodes. The results of this study will provide a more comprehensive understanding of $PM_{2.5}$ pollution control in semi-arid regions.

## 2 Material and methods

### 2.1 Study area and sampling

Hohhot (40°51′ – 41°8′ N, 110°46′ – 112°10′ E) is located in the northern part of the North China Plain and the central part of Inner Mongolia Autonomous Region. It is a core city of the Hohhot-Baotou-Ordos urban agglomeration, with an area of 17,224 $km^2$ and 3,496,000 inhabitants (http://www.tjcn.org/tjgb/05nmg/37047.html). Topographically, it is in the alluvial lake basin between the Yinshan Mountains and the Yellow River, with Daqing Mountains in the north and Manhan Mountain in the southeast. Hohhot has a typical semi-arid climate, with a mean annual precipitation of 335.2–534.6 mm, which occurs mainly in summer. Due to the minimal precipitation and dry continental terrain, frequent dust storms occur in spring. It has six months of coal-fired heating period ($15^{th}$ October–$15^{th}$ April the next year). The sampling site was located on the rooftop of the main building of the Ecological

and Environmental Department of the Inner Mongolia autonomous region (Figure 1) and represents a typical semi-arid urban environment.

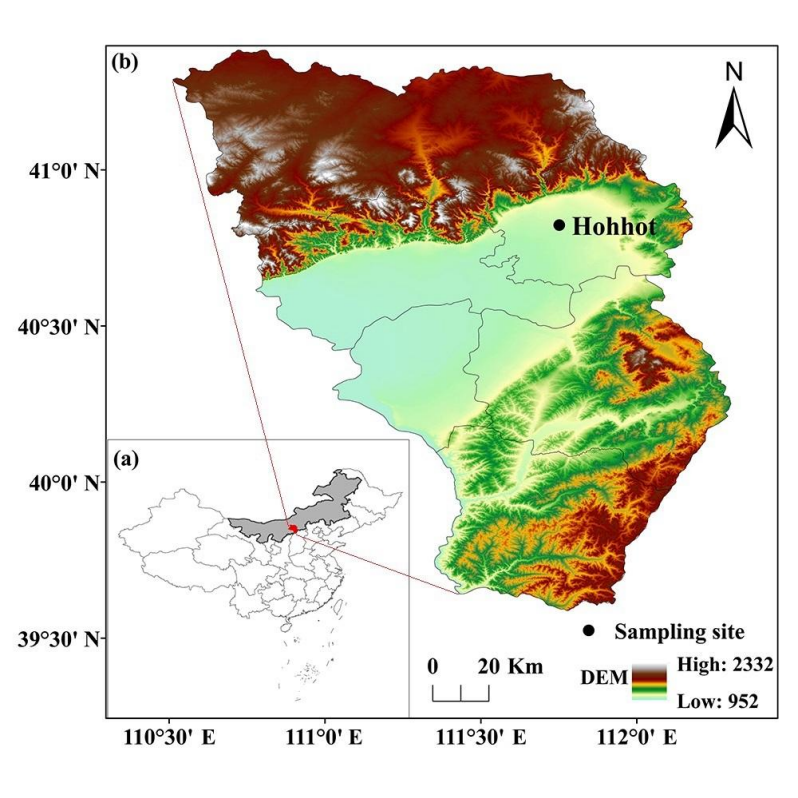


**Figure 1.** Location of (a) Hohhot in China, and (b) the sampling site in Hohhot

The 23-h (10:00 to 09:00 the next day) $PM_{2.5}$ samples were collected in parallel on quartz filters (Pallflex Tissuquartz™, 90 mm, USA) and polypropylene filters (Beijing Safelab Technology Ltd., 90 mm, China) using medium volume air samplers (Model 2050, Qingdao Laoshan Applied Technology Research Institute, China) with a flow rate of 100 L/min. The quartz filters were used for the analysis of water-soluble ions (WSIs) and carbonaceous aerosols (OC and EC), while polypropylene filters were used for inorganic elements. A total of 722 $PM_{2.5}$ samples (361 quartz and 361 polypropylene filters) were collected from 8$^{th}$ October, 2019 to 7$^{th}$ October, 2020. Before and after sampling, the quartz filters and polypropylene filters were conditioned for at least 24 h at a stable temperature (20 ± 1 ℃) and relative humidity (50 ± 5%) and then weighed using a microbalance (CP225D, Sartorius, Germany), with a sensitivity of ± 0.01 mg. After weighing, all of the filters were stored at -18 ℃ until analysis. The online hourly concentrations of gaseous pollutants ($SO_2$, $NO_2$, CO, and $O_3$) were collected at the same site. In addition, the hourly meteorological variables, including relative humidity (RH), wind speed (WS), wind direction (WD), ambient temperature (T), and atmospheric pressure (P) were observed synchronously using an automatic weather station (WS500-UMB, Lufft, Germany).

### 2.2 Chemical analysis

The water-soluble ions (WSIs, including $SO_4^{2-}$, $NO_3^-$, $NH_4^+$, $Cl^-$, $F^-$, $K^+$, $Ca^{2+}$, $Na^+$, and $Mg^{2+}$) were

determined using ion chromatography (Metrohm 881Compact IC Pro, Switzerland). The organic carbon and elemental carbon (EC) were analyzed using a thermal/optical carbon analyzer (DRI Model 2001, Atmoslytic Inc., USA) following the IMPROVE_A protocol (Chow et al., 2007; Cao et al., 2005). The detailed descriptions of the procedures for WSIs and carbonaceous aerosols can be found in our previous studies (Zhou et al., 2018; Zhou et al., 2016). The inorganic elements, including Si, Al, S, Cl, K, Ca, Ti, V, Cr, Mn, Fe, Cu, Zn, Co, and Pb were analyzed by energy dispersive X-ray fluorescence spectroscopy (Epsilon5, PANalytical B.V., Netherlands) according to the National Environmental Protection standard method of China (HJ 829-2017) and previous studies (Dao et al., 2022; Dao et al., 2021; Chiari et al., 2018). Field blank and replicate analyses were carried out once per 10 samples. The concentrations of field blanks were all lower than the method detection limits, and the relative deviations of replicate analyses were < ~ 5%. All the analytical procedures were strictly controlled according to the referred methods to reduce artificial interference.

### 2.3. Data analysis

The organic matter (OM) and mineral dust (MD) were calculated using the following equations (1 - 2). To estimate the secondary formation of inorganic and organic aerosols, the sulfur oxidation ratio (SOR), nitrogen oxidation ratio (NOR), and secondary organic carbon (SOC) were calculated using the following equations (3 - 5) (Xie et al., 2019; Liu et al., 2021):

$$OM = 1.6 \times [OC] \quad (1)$$

$$MD = 2.14 \times [Si] + 1.89 \times [Al] + 1.40 \times [Ca] + 1.43 \times [Fe] + 1.58[Mn] + 1.21 \times [K] + 1.67 \times [Ti] \quad (2)$$

$$SOR = [SO_4^{2-}] / ([SO_4^{2-}] + [SO_2]) \quad (3)$$

$$NOR = [NO_3^-] / ([NO_3^-] + [NO_2]) \quad (4)$$

$$SOC = OC - EC \times (OC/EC)_{min} \quad (5)$$

### 2.4 Source apportionment

Positive matrix factorization (PMF, version 5.0) was used to estimate source contributions of $PM_{2.5}$ in Hohhot according to the user guide of the United States Environmental Protection Agency (Norris et al., 2014) and a previous study (Paatero and Tapper, 1994). A total of fifteen dominant species ($SO_4^{2-}$, $NO_3^-$, $NH_4^+$, $K^+$, $Na^+$, $Ca^{2+}$, $Mg^{2+}$, OC, EC, Si, Cl, Ti, Fe, Zn, and Pb) were used as input files for the PMF modeling. The displacement (DISP) and bootstrap (BS) methods were conducted to estimate the uncertainty and rotational ambiguity of PMF solutions (Paatero et al., 2014). According to the changes in $Q/Q_{expected}$ and estimation diagnostics analysis, six factors solutions were selected. All of the factors showed a BS mapping above 80 %. The decreased Q values were lower than 0.1 %, and no factor swap occurred. The results indicate that the BS uncertainties can be fully interpreted and the selected solutions were sufficiently robust (Tian et al., 2020; Wang et al., 2021). The summary of error estimation diagnostics from BS and DISP are shown in Tables S1–S8. The source profiles of $PM_{2.5}$ are shown in Figures S1–S8.

## 3 Results and discussion

### 3.1 Temporal variation in $PM_{2.5}$ and chemical composition

The daily concentration of $PM_{2.5}$ varied dynamically from 4.0 to 293.8 μg/m$^3$, with an annual mean concentration (± standard deviation) of 42.6 ± 40.2 μg/m$^3$, which is higher than the annual mean concentration limits (35 μg/m$^3$) of the National Ambient Air Quality Standards (NAAQS, GB 3095-2012). There were 51 daily $PM_{2.5}$ concentrations higher than the 24-h average concentration limit (75 μg/m$^3$) of NAAQS, accounting for 14.1% of the total number of sampling days. Furthermore, most of them occurred in the heating period, particularly with a predominant wind direction from the southeast. The high intensity of coal combustion for heating discharges a large number of gaseous pollutants ($SO_2$, $NO_2$, and CO), coupled with unfavorable meteorological conditions (high RH and low WS; Figure 2a, 2b), lead to the rapid accumulation of air pollutants (Figure 2c, 2d).

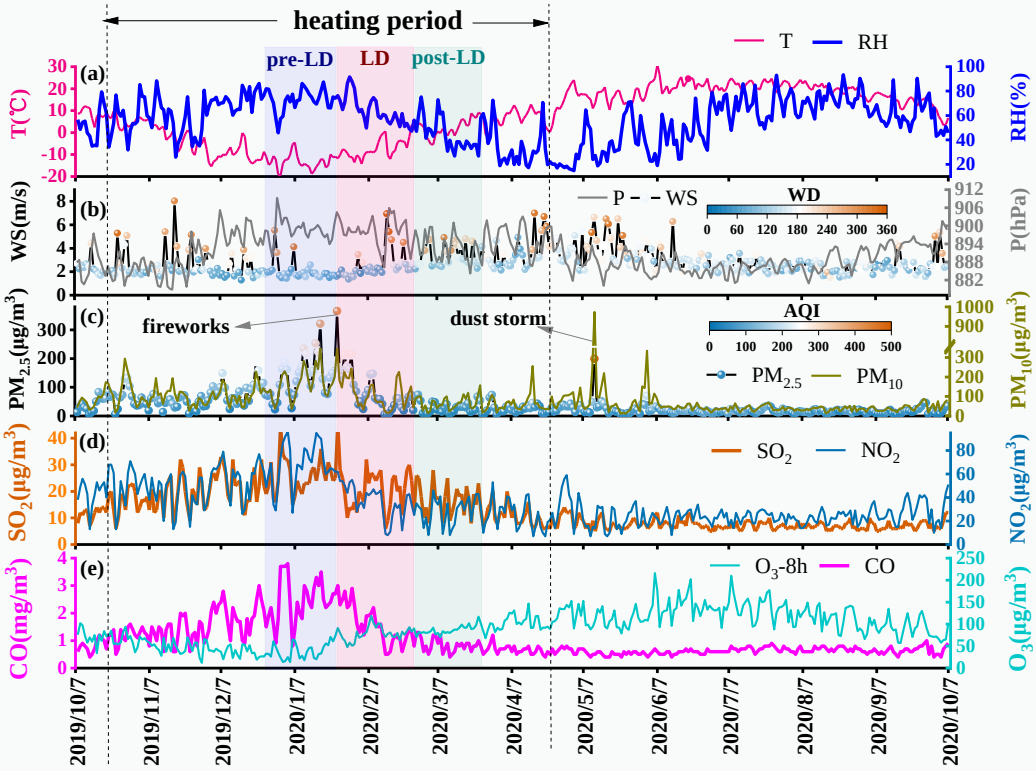


**Figure 2.** Daily variations in atmospheric pollutants and meteorological variables in Hohhot during the sampling period from 8$^{th}$ October, 2019 to 7$^{th}$ October, 2020. The blue, red, and green backgrounds represent the pre-lockdown, lockdown, and post-lockdown periods, respectively. T, RH, WS, WD, P, and AQI represent the ambient temperature, relative humidity, wind speed, wind direction, atmospheric pressure, and air quality index, respectively.

During haze episodes, a substantial increase in secondary inorganic components (sulfate, nitrate, and ammonium, SNA) was observed (Figure 3a–3c). The rapid increase in SNA was the main driving factor behind the increase in $PM_{2.5}$. High RH is conducive to the secondary formation of sulfates and nitrates,

presenting higher SOR and NOR in these pollution periods (Figure 3a, 3b). In the heating period, in addition to the contribution of SNA to $PM_{2.5}$, the primary pollutants such as $Cl^-$ ($p < 0.001$) and EC ($p < 0.001$) were higher than those in the non-heating period (Figure 3d, 3e). Hohhot is an inland city, basically unaffected by sea salt. Furthermore, a higher average $Cl^-/Na^+$ ratio (3.43 for January) suggests the presence of non-marine anthropogenic sources of chloride. Chloride is mainly emitted from coal combustion facilities in Hohhot, especially during the heating period. It can be used as an auxiliary marker of coal combustion in Hohhot. Higher SOR was observed in winter and summer in Hohhot (Figure 3a). High SOR in winter is mainly caused by heterogeneous processes under high RH conditions, while that in summer is caused by homogeneous gas-phase oxidation reactions under high temperatures and $O_3$ concentrations (Zhang et al., 2018; Li et al., 2017a). NOR was higher in winter, whereas it was lower in summer (Figure 3b). The higher NOR in winter can be ascribed to the rapid formation of nitrate under high RH. The lower NOR in summer may be related to the high temperature, which is favorable for nitrate volatilization (Daher et al., 2012). The higher SOR and NOR in winter indicate the higher secondary formation of sulfate and nitrate that resulted the heavy pollution episodes in pre-LD and LD periods.

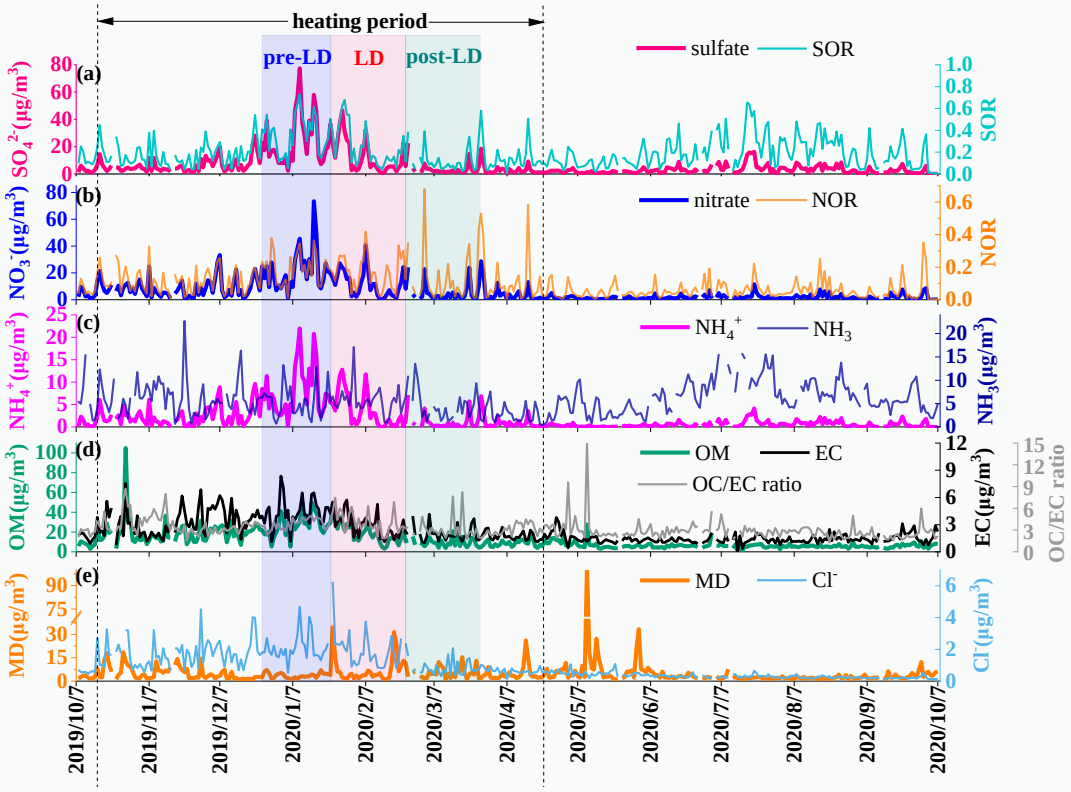


**Figure 3.** Daily variations in chemical composition of $PM_{2.5}$, SOR, NOR, $NH_3$, and OC/EC ratio in Hohhot during the sampling period. The blue, red, and green background represent the pre-lockdown, lockdown, and post-lockdown periods, respectively. OM, MD, SOR, and NOR represent the organic matter, mineral dust, sulfur oxidation ratio, and nitrogen oxidation ratio, respectively.

Hohhot initiated a Level-I public health emergency response control action on 25th January, 2020 and downgraded it to a Level-III response on 25th February, 2020. During this period, complete lockdown

measures were taken to prevent the transmission of the SARS-CoV-2. In order to estimate the impacts of lockdown measures on the air quality, we compared the atmospheric pollutants during pre-LD period ($25^{th}$ December, 2019 to $24^{th}$ January, 2020), LD period ($25^{th}$ January, 2020 to $24^{th}$ February, 2020), and post-LD period ($25^{th}$ February, 2020 to $24^{th}$ March, 2020). The comparison of atmospheric pollutants ($PM_{2.5}$, $PM_{10}$, $SO_2$, $NO_2$, $O_3$, and CO) between the LD period and the same period in 2017–2019 are shown in Figure S9. The average concentrations of $PM_{2.5}$, $PM_{10}$, $O_3$, and CO increased by 77.8% ($p < 0.01$), 34.6% ($p < 0.05$), 14.5% ($p < 0.001$), and 5.9% ($p < 0.001$), respectively, whereas the average concentrations of $SO_2$ and $NO_2$ decreased by 43.2% ($p < 0.05$) and 8.6% ($p < 0.001$), respectively.

The annual mean concentration of OM, $SO_4^{2-}$, $NO_3^-$, MD, EC, $NH_4^+$, and $Cl^-$ were 12.1, 6.6, 6.4, 4.9, 2.2, 2.0, and 1.1μg/m$^3$ (Figure 4a), accounting for 31.5%, 13.4%, 12.3%, 14.2%, 6.6%, 3.3%, and 2.5% of $PM_{2.5}$, respectively (Figure 4b). Compared with the result of Hohhot in 2014 − 2015(Wang et al., 2019), the annual mean concentration of $NO_3^-$ increased, whereas the concentration of the other species decreased (Figure S10a). Due to the implemented measures, a sharp decrease in OM and MD was observed, resulting in a considerable decrease in $PM_{2.5}$ (decreased from 66μg/m$^3$ in 2014 − 2015 to 42.6μg/m$^3$ in 2019 − 2020). The proportion of $SO_4^{2-}$, $NO_3^-$, and OM increased considerably, whereas the proportion of MD showed a substantial decrease (Figure S10b). The result indicates that the contribution of chemical composition related to secondary formation has increased in recent years. However, the proportion of MD was still substantially higher than those of other cities in South China (Huang et al., 2013), southwest China (Feng et al., 2021), southeast China (Li et al., 2017b), and the Central Plains Urban Agglomeration (Liu et al., 2019), which is close to the cities in northern China (Liu et al., 2021; Xie et al., 2019) and northwest China (Zhou et al., 2021). The lower relative humidity, higher wind speed, and larger area of uncovered surface soil lead to frequent dust storms in semi-arid regions, resulting in a higher contribution of MD than in the humid area. The result indicates that the cities in arid or semi-arid regions (such as in northern China and northwest China) are more susceptible to mineral dust sources. The monthly average concentrations of SNA and OM during the heating period ($15^{th}$ October to $15^{th}$ April next year), especially in January, were higher than those of other non-heating months (Figure 4a), which were related to the coupled effect of a large amount of atmospheric precursors ($SO_2$, $NO_2$, and volatile organic compounds) and unfavorable meteorological conditions (high RH and low WS; Figure S11). Due to the frequent dust storms, the average concentration of MD in May (9.4 μg/m$^3$) was considerably higher than that of other months, accounting for 21.8% of $PM_{2.5}$ mass. The relatively high proportion of sulfates in August may be caused by its higher SOR, which is enhanced by photochemistry under high T, strong solar radiation, and high RH conditions.

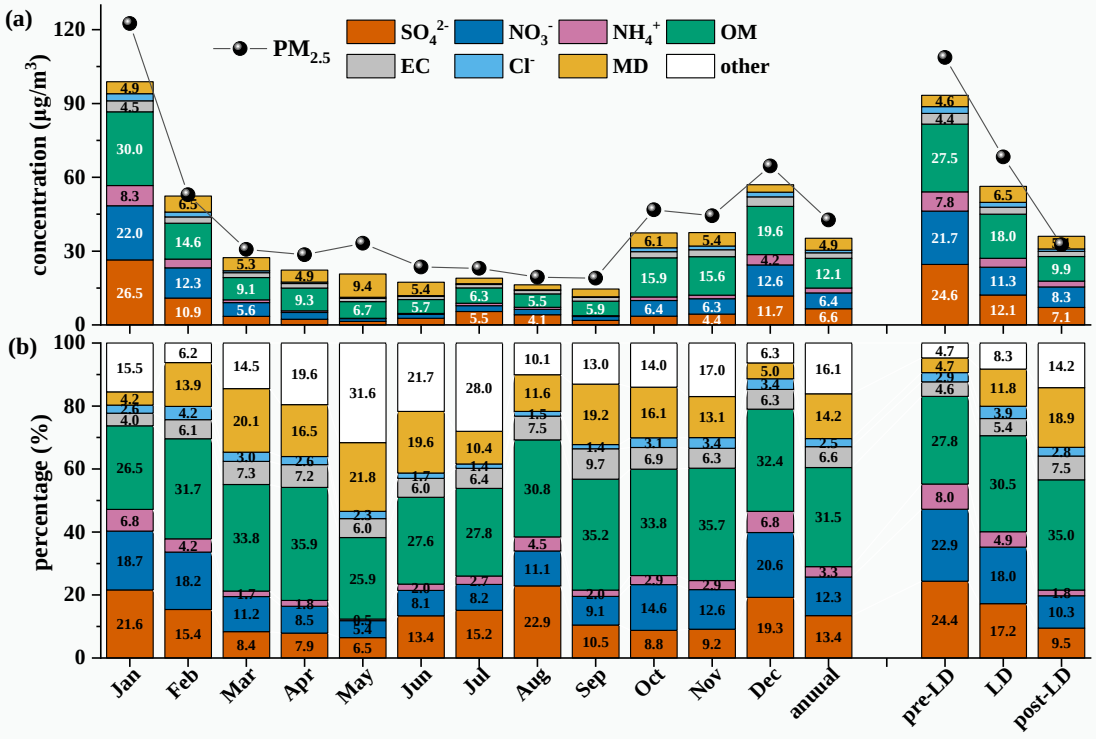


**Figure 4.** Monthly variation in (a) concentrations and (b) percentages of chemical components of $PM_{2.5}$ in Hohhot during the sampling period. Pre-LD, LD, and post-LD represent the pre-lockdown, lockdown, and post-lockdown periods, respectively. OM and MD represent organic matter and mineral dust, respectively.

The OM, sulfate, nitrate, and ammonium were the predominant components of $PM_{2.5}$ during the pre-LD period (25$^{th}$ December, 2019 to 24$^{th}$ January, 2020), accounting for 27.8, 24.4, 22.9, and 8.0% of $PM_{2.5}$ mass, respectively (Figure 4). During this period, the SNA contributed 55.3% by to the total $PM_{2.5}$, slightly higher than those of the cities in northern China such as Xi'an (50.0%) (Tian et al., 2021) and Beijing (48.5%) (Ren et al., 2021), and lower than the cities in southern China such as Guangzhou (78.7%) (Wang et al., 2021), Nanjing (68.2%) (Ren et al., 2021), and Shanghai (75.4%) (Chen et al., 2020). Sulfate was the predominant component of SNA in Hohhot during this period, whereas nitrite was the main contributor to SNA in Guangzhou, Nanjing, and Shanghai. The result indicated that higher SNA contributions in megacities of southern China are mainly related to vehicular emission. The higher contribution of sulfate in Hohhot is mainly related to coal combustion for winter heating. OM contributed by 27.8% to the total $PM_{2.5}$, lower than that of Xi'an (42.0%) (Tian et al., 2021), and higher than that of the other cities listed in Table S9. The contribution of EC is higher than all of the cities listed in Table S9. The higher contribution of sulfate, OM and EC in Hohhot indicated that coal combustion may have been a predominant source of $PM_{2.5}$ during the pre-LD period. Most studies listed in Table S9 used online data, from which it is not possible to calculate the contribution of MD. However, our offline data showed that MD contributed by 11.8% and 14.2% to the total $PM_{2.5}$ during the LD period and for the whole sampling year, indicating that MD is one of the main contributors of $PM_{2.5}$ that has been neglected in previous

studies. The proportion of chemical species ranked as OM (27.8%) > $SO_4^{2-}$ (24.4%) > $NO_3^-$ (22.9%) > $NH_4^+$ (8.0%) > MD (4.7%) > EC (4.6%) > $Cl^-$ (2.9%), OM (30.5%) > $NO_3^-$ (18.0%) > $SO_4^{2-}$ (17.2%) > MD (11.8%) > EC (5.4%) > $NH_4^+$ (4.9%) > $Cl^-$ (3.9%), and OM (35.0%) > MD (18.9%) > $NO_3^-$ (10.3%) > $SO_4^{2-}$ (9.5%) >EC (7.5%) > $Cl^-$ (2.8%) > $NH_4^+$ (1.8%) during the pre-LD, LD, and post-LD periods, respectively. Compared with the pre-LD period, the concentration of sulfate ($p < 0.01$), nitrate ($p < 0.01$), ammonium ($p < 0.01$), OM ($p < 0.001$), and EC ($p < 0.001$) decreased substantially due to the decline in the emission intensity under the strict control measures during the LD period (Figure 4a, Table S10). The percentage of sulfate (not significant for LD and $p < 0.01$ for post-LD), nitrate (not significant for LD and $p < 0.05$ for post-LD), and ammonium ($p < 0.05$ for LD and $p < 0.01$ for post-LD) decreased continuously during LD and post-LD, while the MD ($p < 0.01$ for LD and $p < 0.001$ for post-LD), OM (not significant for both two periods), and EC (not significant for LD and $p < 0.01$ for post-LD) increased (Table S10). The mean value of RH declined continuously from pre-LD to LD and post-LD, while the mean value of WS showed an opposite trend (Figure S11). The lower RH and higher WS were not conducive to the secondary formation and accumulation of SNA. Therefore, due to the emission reduction and improved atmospheric conditions, the proportion of SNA decreased sufficiently (from 55.3% in pre-LD to 40.1% in LD and 21.6% in post-LD). The atmospheric diffusion conditions improved during the post-LD period, and the concentration of OM, SNA, EC, and $Cl^-$ decreased substantially. These results suggest that the substantial changes that occurred in source contributors after the COVID-19 outbreak resulted in dramatic changes to aerosol composition.

To elucidate the rapid increase in $PM_{2.5}$, the sampling days were divided into four categories according to the daily concentration of $PM_{2.5}$: clean (CP, $PM_{2.5} < 35$ μg/m$^3$), slightly polluted (SP, $35 \leq PM_{2.5} < 75$ μg/m$^3$, moderately polluted (MP, $75 \leq PM_{2.5} < 150$ μg/m$^3$, and heavily polluted (HP, 150μg/m$^3$ $\leq PM_{2.5}$). The values of 24$^{th}$ January, 2020 (Chinese New Year's Eve) and 11$^{th}$ May, 2020 (a dust storm day) were excluded from the HP analysis. These two heavy pollution days were analyzed separately as two types, namely fireworks and dust storm. The meteorological conditions, gaseous precursors, and chemical composition of different pollution levels and types are shown in Figure 5. The concentrations of OM, sulfate, nitrate, and ammonium were in the order of CP < SP < MP < HP.

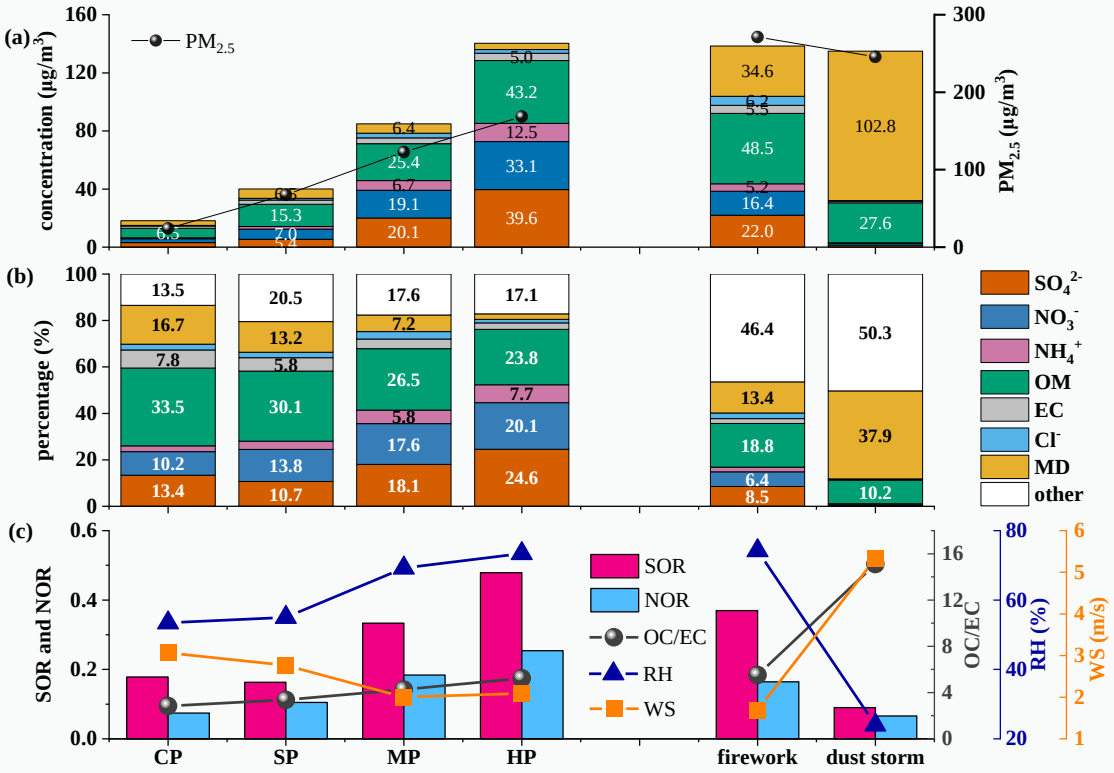


**Figure 5.** (a) Concentrations and (b) percentages of chemical components in $PM_{2.5}$, (c) meteorological conditions, SOR, NOR, and OC/EC at different pollution levels and during different types of pollution events. CP, SP, MP, and HP represent the clean ($PM_{2.5}$ < 35 μg/m$^3$), slightly polluted (35 ≤ $PM_{2.5}$ < 75 μg/m$^3$), moderately polluted (75 ≤ $PM_{2.5}$ < 150 μg/m$^3$, and heavily polluted periods (150μg/m$^3$ ≤ $PM_{2.5}$), respectively.

From CP to HP, the percentages of SNA increased (from 26.1% to 52.4%), whereas the percentages of OM and MD decreased (from 33.5% to 23.8%, and from 16.7 to 2.4, respectively). This response is related to the adverse meteorological conditions characterized by high RH and low WS, leading to the enhanced formation of SNA (higher SOR and NOR). The values of SOR increased from 0.18 during CP to 0.48 during HP. The values of NOR increased from 0.07 during CP to 0.25 during HP. The results suggest enhanced SNA formation during heavy pollution episodes. The coupled effects of high RH and low WS promoted the rapid increase of fine particulate matter on haze days in Hohhot. The high WS is beneficial for the elimination of atmospheric pollutants, resulting in low concentrations of $SO_2$ and $NO_2$ on dust storm days. Furthermore, the low RH is detrimental to the secondary formation of SNA (lower SOR and NOR), resulting in a lower SNA content in dust storm days. MD and OM contribute 102.8 and 27.6 μg/m$^3$ to $PM_{2.5}$ during dust storm days, accounting for 37.9% and 10.2% of $PM_{2.5}$, respectively. The proportion of MD was highest in dust storm days, mainly because of the relatively high WS and low RH that were conducive to the re-suspension of crustal dust. During Lunar New Year, fireworks discharge a large number of gaseous pollutants, coupled with low WS and high RH, the concentrations of SNA, OM, and EC increased rapidly, resulting in serious pollution.

### 3.2 Factors influencing $PM_{2.5}$

The correlations between the chemical composition of $PM_{2.5}$, meteorological variables, and air pollutants are shown in Figure 6. $PM_{2.5}$ was negatively correlated with $O_3$, T, and WS at $p < 0.001$, indicating that high WS was beneficial for the elimination of fine particulate matter, while $O_3$ and T were mainly related to seasonal variation in sources and meteorological conditions. $PM_{2.5}$ was positively correlated with most of the aerosol components and gaseous pollutants, indicating that the source of $PM_{2.5}$ was very complex and influenced by a variety of factors. The SNA in $PM_{2.5}$ was positively correlated with RH ($p < 0.001$), indicating that high RH promotes heterogeneous formation of SNA.

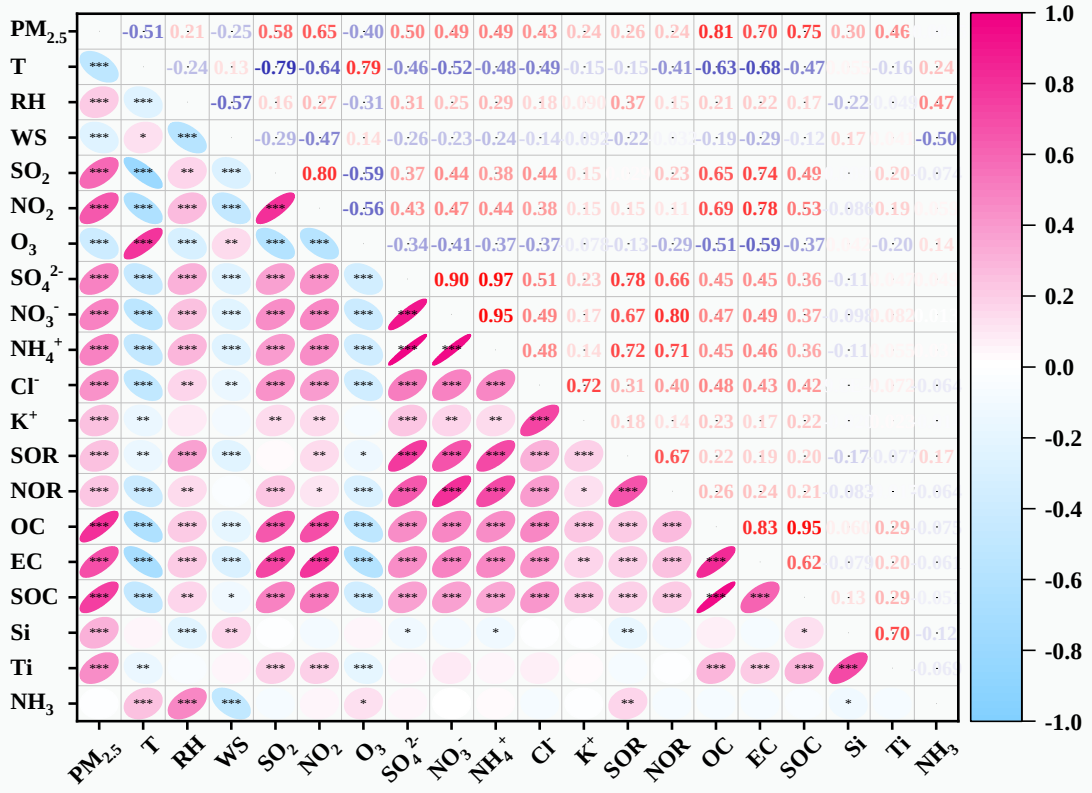


**Figure 6.** Correlation between chemical components of $PM_{2.5}$, meteorological variables, SOR, NOR, and air pollutants in Hohhot during the sampling period (* $p < 0.05$， ** $p < 0.01$， *** $p < 0.001$).

The results suggest that RH played a vital role in the formation of haze by accelerating the conversion of $SO_2$ to $SO_4^{2-}$ and $NO_2$ to $NO_3^-$, deteriorating the air quality. NOR was negatively correlated with T at $p < 0.001$, which may be related to the volatility of $NH_4NO_3$. The higher T is favorable for nitrate volatilization, resulting in lower NOR (He et al., 2012). SOR and NOR was positively correlated with RH at $p < 0.001$ and $p < 0.05$, respectively, suggesting that both SOR and NOR were influenced by RH. The higher transformation of $SO_2$ to SNA was negatively correlated with WS ($p < 0.001$), indicating that high WS was conducive to the rapid elimination of SNA. SNA and its gaseous precursors ($SO_2$ and $NO_2$) were positively correlated ($p < 0.001$) but not related to $NH_3$, indicating that the formation of SNA was mainly controlled by $SO_2$ and $NO_2$ rather than $NH_3$. The carbonaceous aerosols (OC, EC, and SOC)

were positively correlated with $Cl^-$, SNA, $SO_2$, and $NO_2$ ($p < 0.001$), which are mainly affected by their common source in coal, used in heating. Silicon was positively correlated with WS ($p < 0.01$), indicating that high WS is beneficial to the re-suspension of soil or dust, resulting in an increase in Si in $PM_{2.5}$. Silicon was negatively correlated with RH ($p < 0.001$), which was related to high WS and low RH in dust storm days.

### 3.3 Source apportionment of $PM_{2.5}$

The sources of $PM_{2.5}$ were apportioned using the PMF model (EPA PMF 5.0). The results of the source apportionment during different sampling periods are shown in Figure 7 and summarized in Table S11. The $PM_{2.5}$ concentrations in spring, summer, autumn, winter, and annually were 32.4, 24.3, 37.0, 80.8, 42.6 μg/m$^3$, respectively. Coal combustion (CC), vehicular exhaust (VE), crustal sources (CS), and secondary inorganic aerosols (SIA) were the main contributors to $PM_{2.5}$ over the sampling year, contributing 38.3%, 35.0%, 13.5%, and 11.4% to $PM_{2.5}$, respectively. The contribution of primary sources such as CC, VE, and dust source (refer to the sum of construction dust and crustal sources in this study) in Hohhot was higher than the megacities such as Beijing (Z ƙov áet al., 2016), Tianjin (Tian et al., 2021), and Shanghai (Feng et al., 2022), whereas the SIA and BB contributions were lower than in these cities (Table S11). The result indicates that the contribution of secondary aerosols is predominant in megacities, while the primary source is predominant in semi-arid regions. Therefore, the control of primary sources is an effective way to reduce the concentration of $PM_{2.5}$ in Hohhot.

The CC contribution to $PM_{2.5}$ in spring, summer, autumn, and winter was 14.6, 5.7, 12.4, and 41.3 μg/m$^3$, with a contribution percentage of 56.1%, 24.0%, 38.9%, and 65.4%, respectively. Coal combustion was the main contributor to $PM_{2.5}$ in Hohhot, especially during the heating period. Summer is the only season for completely no coal-fired heating, a relatively low contribution of CC was observed in summer. The VE contribution concentrations in spring, summer, autumn, and winter were 4.4, 11.5, 10.7, and 9.0 μg/m$^3$, contributing 17.0%, 48.4%, 33.8%, and 14.3% to $PM_{2.5}$, respectively. The peak seasonal contribution percentage of VE was observed in summer. This is mainly attributable to a substantial decline in the contribution of other sources, increasing the proportion of VE. The contribution concentration of SIA followed the order of winter (6.6 μg/m$^3$) > autumn (3.5 μg/m$^3$) > summer (1.2 μg/m$^3$) > spring (1.1 μg/m$^3$), with a contribution percentage of 10.5%, 11.1%, 5.3%, and 4.2%, respectively. The higher contribution of SIA can be attributed to the large amount of gaseous precursors emitted by CC in winter, whereas the higher SIA contribution in autumn was related to the high oxidation rate. A relatively low contribution was observed in spring. The lower contribution of SIA in spring may be related to the high WS and low RH, which is unfavorable for SNA formation and accumulation.

The contributions concentrations of CS followed the order of spring (4.9 μg/m$^3$) > autumn (4.4 μg/m$^3$) > winter (4.3 μg/m$^3$) > summer (3.2 μg/m$^3$), with a contribution percentage of 18.6%, 13.8%, 6.8%, and 13.5%, respectively. A relatively high contribution of CS to $PM_{2.5}$ was observed in spring, which is associated with the increased long-range transportation of crustal sources due to dry and windy weather in Hohhot. The higher contribution of dust sources to $PM_{2.5}$ has been reported in some other

semi-arid regions, such as Guanzhong basin (Li et al., 2022) and Lanzhou (Liang et al., 2019), indicating that the semi-arid regions are more susceptible to dust sources. The source apportionment results indicate that primary sources such as CC, VE, and dust sources in Hohhot were predominant, which is different from cities with high secondary pollution.

During the LD period, the contribution of SIA, CC, CS, BB, CD, and VE was 22.6, 18.2, 7.7, 5.6, 3.0, and 2.6 μg/m$^3$ to $PM_{2.5}$, respectively, accounting for 37.8%, 30.5%, 12.9%, 9.4%, 5.1%, and 4.4% of the total $PM_{2.5}$ mass (Figure 7). The contribution of CC and dust source (the sum of CS and CD) during the LD period in Hohhot was much higher than those of Tangshan (Wang et al., 2021), Taiyuan (Wang et al., 2022), and Xiamen (Hong et al., 2021) (Table S11). The contribution of SIA was lower than Tangshan and Taiyuan, while higher than Xiamen. Hohhot, Tangshan, and Taiyuan are located in northern China, and consume large amount of coal for winter heating. The high intensity of gaseous precursors emitted from coal combustion is reasonable for a high contribution of SIA. The contribution of VE in Hohhot was lower than Xiamen and Taiyuan. The contribution of VE decreased from 35.5% to 4.4%, whereas the SIA increased from 21.1 % to 37.8 %. The substantial reduction in VE was associated with the strict traffic restrictions during the LD period, which is consistent with the findings in Taiyuan (Wang et al., 2022). Compared with the LD period, the contribution of VE increased from 4.4% to 14.7% during the post-LD period, which can be ascribed to the canceled traffic restrictions. The contribution of CC increased from 30.5% during the LD period to 68.7% during the post-LD period, while the concentration decreased from 29.2 to 18.2 μg/m$^3$. The contribution of SIA decreased from 37.8% during the LD period to 5.0% during the post-LD period, which can be attributed to the improved atmospheric conditions.

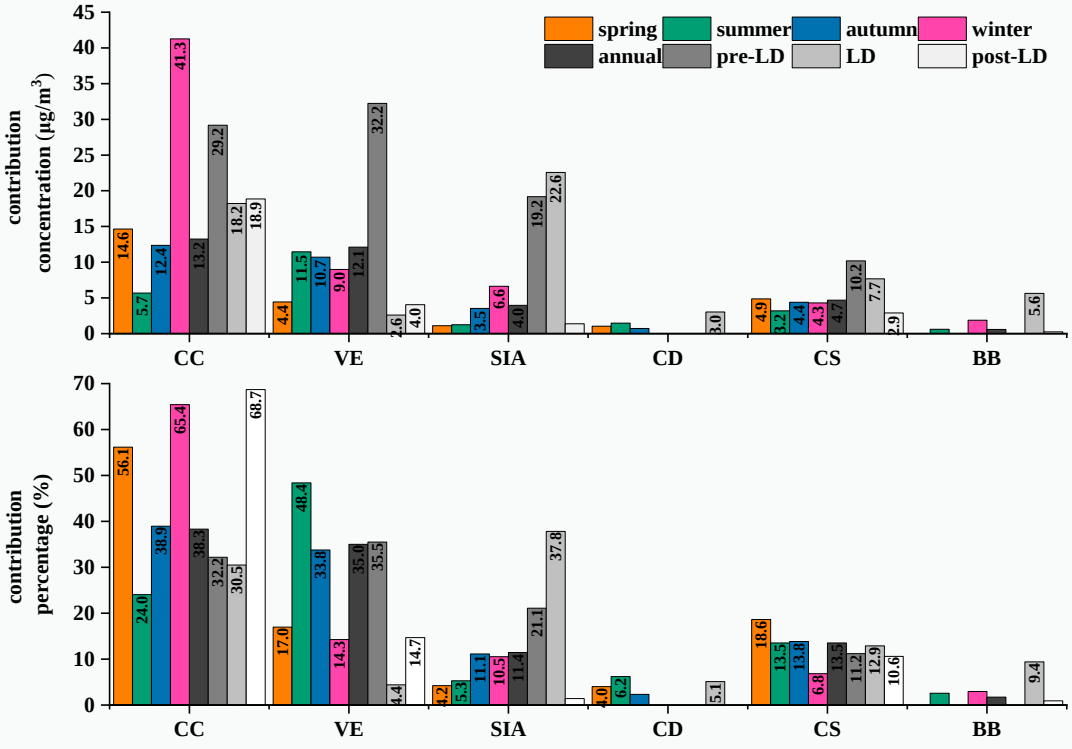

**Figure 7.** (a) Concentration and (b) percentage of source contribution to $PM_{2.5}$ in Hohhot in spring, summer, autumn, winter, over the sampling year, pre-lockdown, lockdown, and post-lockdown periods. CC, VE, SIA, CD, CS, and BB represent coal combustion, vehicular emission, secondary inorganic aerosol, construction dust, crustal sources, and biomass burning, respectively.

## 4 Conclusion

A single year's offline measurement was conducted in Hohhot to reveal the chemical characteristics and sources of $PM_{2.5}$ in a semi-arid region. Organic matter, mineral dust, sulfate, and nitrite were the predominant components of $PM_{2.5}$ in Hohhot, and coal combustion, vehicular emission, crustal sources, and secondary inorganic aerosols were the main contributors to $PM_{2.5}$. The high proportion of mineral dust composition and higher contribution of crustal sources to $PM_{2.5}$ indicated that cities in semi-arid regions are more susceptible to dust sources. The heavy pollution in winter can be attributed to the rapid increase of SNA under high RH and low WS conditions, while the heavy pollution in spring was associated with long-range transmission of crustal sources due to the dry and windy weather. Compared with the pre-LD period, the concentration of SNA, OM, and EC decreased substantially during LD and post-LD periods due to the lockdown measures.. The source contribution of secondary inorganic aerosols and vehicular emission decreased during the lockdown period, whereas coal combustion increased. The substantial reduction in the contribution of vehicular emissions was associated with the strict traffic restrictions during the lockdown period, the increase in vehicular emission contributions during the post-lockdown period can be attributed to the canceled traffic restrictions.

A relatively high contribution of primary sources, such as coal combustion and dust source, was observed in Hohhot. Therefore, the control of primary sources, such as increasing the proportion of clean energy to reduce coal consumption, could be an effective way to reduce the concentration of $PM_{2.5}$ in Hohhot. The unfavorable meteorological conditions played an integral role during winter and promoted SNA formation and accumulation, causing frequent heavy pollution events. The reduction in anthropogenic activities and the important role of meteorology in the formation of air pollutants should be considered in aerosol quality and policy measures. The emission reduction of gaseous precursors ($SO_2$ and $NO_x$) under adverse meteorological conditions can prevent heavy pollution events driven by SNA. The control of coal combustion sources and accurate ambient air quality forecasting techniques will do much good to reduce annual concentrations of $PM_{2.5}$ and the occurrence of heavy pollution days, respectively. This study provides new insight for the formulation of effective policies to improve aerosol pollution in semi-arid regions.

*Data availability.* Data are available from the corresponding author upon request (hjzhou@imnu.edu.cn).

*Supplement.* The Supplement related to this article is available online at

*Author Contributions*. HJZ designed the study and prepared the paper with inputs from all the coauthors. Data

analysis and source apportionment were done by HJZ and TL. PL, JWW, and DDGL carried out the experiments. YLT provided the air quality data. FH, BS, and XJZ participated in the field campaign and data analysis. XC and ZQW supervised the study.

*Competing interest.* The authors declare that they have no known competing financial interests or personal relationships that could have appeared to influence the work reported in this paper.

**Acknowledgments.** This work was supported by the National Natural Science Foundation of China (42167015), Natural Science Foundation of Inner Mongolia (2018MS02001), Scientific Research Foundation for the High-level Talents of Inner Mongolia (24), and Scientific Research Foundation for the High-level Talents of Inner Mongolia Normal University (2018YJRC005), Science and Technology Project of Inner Mongolia Autonomous Region (2021GG0406).

## References

Bao, R., and Zhang, A., 2020. Does lockdown reduce air pollution? Evidence from 44 cities in northern China, Science of The Total Environment, 731, 139052, https://doi.org/10.1016/j.scitotenv.2020.139052.

Cao, J. J., Wu, F., Chow, J. C., Lee, S. C., Li, Y., Chen, S. W., An, Z. S., Fung, K. K., Watson, J. G., Zhu, C. S., and Liu, S. X., 2005. Characterization and source apportionment of atmospheric organic and elemental carbon during fall and winter of 2003 in Xi'an, China, Atmospheric Chemistry Physics, 5, 3127-3137, 10.5194/acp-5-3127-2005.

Chang, Y., Huang, R.-J., Ge, X., Huang, X., Hu, J., Duan, Y., Zou, Z., Liu, X., and Lehmann, M. F., 2020. Puzzling haze events in China during the Coronavirus (COVID-19) shutdown, Geophysical Research Letters, 47, e2020GL088533, https://doi.org/10.1029/2020GL088533.

Chen, H., Huo, J., Fu, Q., Duan, Y., Xiao, H., and Chen, J., 2020. Impact of quarantine measures on chemical compositions of $PM_{2.5}$ during the COVID-19 epidemic in Shanghai, China, Science of The Total Environment, 743, 140758, https://doi.org/10.1016/j.scitotenv.2020.140758.

Chiari, M., Yubero, E., Calzolai, G., Lucarelli, F., Crespo, J., Galindo, N., Nicolás, J. F., Giannoni, M., and Nava, S., 2018. Comparison of PIXE and XRF analysis of airborne particulate matter samples collected on Teflon and quartz fibre filters, Nuclear Instruments and Methods in Physics Research Section B: Beam Interactions with Materials and Atoms, 417, 128-132, https://doi.org/10.1016/j.nimb.2017.07.031.

Chow, J. C., Watson, J. G., Chen, L. W. A., Chang, M. C. O., Robinson, N. F., Trimble, D., and Kohl, S., 2007. The IMPROVE_A temperature protocol for thermal/optical carbon analysis: Maintaining consistency with a long-term database, Journal of the Air & Waste Management Association, 57, 1014-1023, 10.3155/1047-3289.57.9.1014.

Clemente, Á., Yubero, E., Nicolás, J. F., Caballero, S., Crespo, J., and Galindo, N., 2022. Changes in the concentration and composition of urban aerosols during the COVID-19 lockdown, Environmental Research, 203, 111788, https://doi.org/10.1016/j.envres.2021.111788.

Collivignarelli, M. C., Abbà, A., Bertanza, G., Pedrazzani, R., Ricciardi, P., and Carnevale Miino, M., 2020. Lockdown for CoViD-2019 in Milan: What are the effects on air quality?, Science of The Total Environment, 732, 139280, https://doi.org/10.1016/j.scitotenv.2020.139280.

Daher, N., Ruprecht, A., Invernizzi, G., De Marco, C., Miller-Schulze, J., Heo, J. B., Shafer, M. M., Shelton, B. R., Schauer, J. J., and Sioutas, C., 2012. Characterization, sources and redox activity of fine and coarse particulate matter in Milan, Italy, Atmospheric Environment, 49, 130-141, https://doi.org/10.1016/j.atmosenv.2011.12.011.

Dao, X., Ji, D., Zhang, X., He, J., Meng, X., Wang, Z., Liu, Y., Xu, X., Tang, G., and Wang, Y., 2021. Characteristics, sources and health risk assessment of $PM_{2.5}$ in China's coal and coking heartland: Insights gained from the regional observations during the heating season, Atmospheric Pollution Research, 12, 101237, https://doi.org/10.1016/j.apr.2021.101237.

Dao, X., Di, S., Zhang, X., Gao, P., Wang, L., Yan, L., Tang, G., He, L., Krafft, T., and Zhang, F., 2022. Composition and sources of particulate matter in the Beijing-Tianjin-Hebei region and its surrounding areas during the heating season, Chemosphere, 291, 132779, https://doi.org/10.1016/j.chemosphere.2021.132779.

Ding, J., Dai, Q., Li, Y., Han, S., Zhang, Y., and Feng, Y., 2021. Impact of meteorological condition changes on air quality and particulate chemical composition during the COVID-19 lockdown, Journal of Environmental Sciences, 109, 45-56, https://doi.org/10.1016/j.jes.2021.02.022.

Feng, X., Tian, Y., Xue, Q., Song, D., Huang, F., and Feng, Y., 2021. Measurement report: Spatiotemporal and policy-related variations of $PM_{2.5}$ composition and sources during 2015–2019 at multiple sites in a Chinese

megacity, Atmospheric Chemistry and Physics, 21, 16219-16235, https://doi.org/10.5194/acp-21-16219-2021.
Feng, X., Feng, Y., Chen, Y., Cai, J., Li, Q., and Chen, J., 2022. Source apportionment of $PM_{2.5}$ during haze episodes in Shanghai by the PMF model with PAHs, Journal of Cleaner Production, 330, 129850, https://doi.org/10.1016/j.jclepro.2021.129850.
Gao, C., Li, S., Liu, M., Zhang, F., Achal, V., Tu, Y., Zhang, S., and Cai, C., 2021. Impact of the COVID-19 pandemic on air pollution in Chinese megacities from the perspective of traffic volume and meteorological factors, Science of The Total Environment, 773, 145545, https://doi.org/10.1016/j.scitotenv.2021.145545.
Gao, J., Peng, X., Chen, G., Xu, J., Shi, G.-L., Zhang, Y.-C., and Feng, Y.-C., 2016. Insights into the chemical characterization and sources of $PM_{2.5}$ in Beijing at a 1-h time resolution, Science of The Total Environment, 542, 162-171, https://doi.org/10.1016/j.scitotenv.2015.10.082.
Gkatzelis, G. I., Gilman, J. B., Brown, S. S., Eskes, H., Gomes, A. R., Lange, A. C., McDonald, B. C., Peischl, J., Petzold, A., Thompson, C. R., and Kiendler-Scharr, A., 2021. The global impacts of COVID-19 lockdowns on urban air pollution: A critical review and recommendations, Elementa: Science of the Anthropocene, 9, 00176, https://doi.org/10.1525/elementa.2021.00176.
Gualtieri, G., Brilli, L., Carotenuto, F., Vagnoli, C., Zaldei, A., and Gioli, B., 2020. Quantifying road traffic impact on air quality in urban areas: A Covid19-induced lockdown analysis in Italy, Environmental Pollution, 267, 115682, https://doi.org/10.1016/j.envpol.2020.115682.
He, K., Zhao, Q., Ma, Y., Duan, F., Yang, F., Shi, Z., and Chen, G., 2012. Spatial and seasonal variability of $PM_{2.5}$ acidity at two Chinese megacities: insights into the formation of secondary inorganic aerosols, Atmospheric Chemistry and Physics, 12, 1377-1395, 10.5194/acp-12-1377-2012.
Hernández-Paniagua, I. Y., Valdez, S. I., Almanza, V., Rivera-Cárdenas, C., Grutter, M., Stremme, W., García-Reynoso, A., and Ruiz-Suárez, L. G., 2021. Impact of the COVID-19 Lockdown on Air Quality and Resulting Public Health Benefits in the Mexico City Metropolitan Area, Frontiers in Public Health, 9, 10.3389/fpubh.2021.642630.
Hong, Y., Xu, X., Liao, D., Zheng, R., Ji, X., Chen, Y., Xu, L., Li, M., Wang, H., Xiao, H., Choi, S.-D., and Chen, J., 2021. Source apportionment of $PM_{2.5}$ and sulfate formation during the COVID-19 lockdown in a coastal city of southeast China, Environmental Pollution, 286, 117577, https://doi.org/10.1016/j.envpol.2021.117577.
Huang, B., Liu, M., Ren, Z., Bi, X., Zhang, G., Sheng, G., and Fu, J., 2013. Chemical composition, diurnal variation and sources of $PM_{2.5}$ at two industrial sites of South China, Atmospheric Pollution Research, 4, 298-305, https://doi.org/10.5094/APR.2013.033.
Huang, X., Ding, A., Gao, J., Zheng, B., Zhou, D., Qi, X., Tang, R., Wang, J., Ren, C., Nie, W., Chi, X., Xu, Z., Chen, L., Li, Y., Che, F., Pang, N., Wang, H., Tong, D., Qin, W., Cheng, W., Liu, W., Fu, Q., Liu, B., Chai, F., Davis, S. J., Zhang, Q., and He, K., 2021. Enhanced secondary pollution offset reduction of primary emissions during COVID-19 lockdown in China, National Science Review, 8, https://doi.org/10.1093/nsr/nwaa137.
Kanniah, K. D., Kamarul Zaman, N. A. F., Kaskaoutis, D. G., and Latif, M. T., 2020. COVID-19's impact on the atmospheric environment in the Southeast Asia region, Science of The Total Environment, 736, 139658, https://doi.org/10.1016/j.scitotenv.2020.139658.
Kumar, A., and Sarin, M. M., 2009. Mineral aerosols from western India: Temporal variability of coarse and fine atmospheric dust and elemental characteristics, Atmospheric Environment, 43, 4005-4013, https://doi.org/10.1016/j.atmosenv.2009.05.014.
Le, T., Wang, Y., Liu, L., Yang, J., Yung Yuk, L., Li, G., and Seinfeld John, H., 2020. Unexpected air pollution with marked emission reductions during the COVID-19 outbreak in China, Science, 369, 702-706, https://doi.org/10.1126/science.abb7431.
Li, J., Li, J., Wang, G., Ho, K. F., Han, J., Dai, W., Wu, C., Cao, C., and Liu, L., 2022. In-vitro oxidative potential and inflammatory response of ambient $PM_{2.5}$ in a rural region of Northwest China: Association with chemical compositions and source contribution, Environmental Research, 205, 112466, https://doi.org/10.1016/j.envres.2021.112466.
Li, L., Tan, Q., Zhang, Y., Feng, M., Qu, Y., An, J., and Liu, X., 2017a. Characteristics and source apportionment of $PM_{2.5}$ during persistent extreme haze events in Chengdu, southwest China, Environmental Pollution, 230, 718-729, https://doi.org/10.1016/j.envpol.2017.07.029.
Li, M., Hu, M., Du, B., Guo, Q., Tan, T., Zheng, J., Huang, X., He, L., Wu, Z., and Guo, S., 2017b. Temporal and spatial distribution of $PM_{2.5}$ chemical composition in a coastal city of Southeast China, Science of The Total Environment, 605-606, 337-346, https://doi.org/10.1016/j.scitotenv.2017.03.260.
Liang, X., Huang, T., Lin, S., Wang, J., Mo, J., Gao, H., Wang, Z., Li, J., Lian, L., and Ma, J., 2019. Chemical composition and source apportionment of $PM_1$ and $PM_{2.5}$ in a national coal chemical industrial base of the Golden Energy Triangle, Northwest China, Science of The Total Environment, 659, 188-199, https://doi.org/10.1016/j.scitotenv.2018.12.335.
Liu, H., Tian, H., Zhang, K., Liu, S., Cheng, K., Yin, S., Liu, Y., Liu, X., Wu, Y., Liu, W., Bai, X., Wang, Y., Shao, P., Luo, L., Lin, S., Chen, J., and Liu, X., 2019. Seasonal variation, formation mechanisms and potential sources of $PM_{2.5}$ in two typical cities in the Central Plains Urban Agglomeration, China, Science of The Total Environment, 657, 657-670, https://doi.org/10.1016/j.scitotenv.2018.12.068.
Liu, Y., Li, C., Zhang, C., Liu, X., Qu, Y., An, J., Ma, D., Feng, M., and Tan, Q., 2021. Chemical characteristics, source apportionment, and regional contribution of $PM_{2.5}$ in Zhangjiakou, Northern China: A multiple sampling sites observation and modeling perspective, Environmental Advances, 3, 100034,

https://doi.org/10.1016/j.envadv.2021.100034.

Lv, Z., Wang, X., Deng, F., Ying, Q., Archibald, A. T., Jones, R. L., Ding, Y., Cheng, Y., Fu, M., Liu, Y., Man, H., Xue, Z., He, K., Hao, J., and Liu, H., 2020. Source–receptor relationship revealed by the halted traffic and aggravated haze in Beijing during the COVID-19 lockdown, Environmental Science & Technology, 54, 15660-15670, https://doi.org/10.1021/acs.est.0c04941.

Matthias, V., Quante, M., Arndt, J. A., Badeke, R., Fink, L., Petrik, R., Feldner, J., Schwarzkopf, D., Link, E. M., Ramacher, M. O. P., and Wedemann, R., 2021. The role of emission reductions and the meteorological situation for air quality improvements during the COVID-19 lockdown period in Central Europe, Atmospheric Chemmistry and Physics Discussion, 2021, 1-48, https://doi.org/10.5194/acp-2021-372.

MEEC: Bulletin of Ecology and Environment Status of China in 2015 (in Chinese), Ministry of Ecology and Environment of China, Beijing, 2015.

MEEC: Bulletin of Ecology and Environment Status of China in 2020 (in Chinese), Ministry of Ecology and Environment of China, Beijing, 2020.

Mendez-Espinosa, J. F., Rojas, N. Y., Vargas, J., Pachón, J. E., Belalcazar, L. C., and Ramírez, O., 2020. Air quality variations in Northern South America during the COVID-19 lockdown, Science of The Total Environment, 749, 141621, https://doi.org/10.1016/j.scitotenv.2020.141621.

Nakada, L. Y. K., and Urban, R. C., 2020. COVID-19 pandemic: Impacts on the air quality during the partial lockdown in São Paulo state, Brazil, Science of The Total Environment, 730, 139087, https://doi.org/10.1016/j.scitotenv.2020.139087.

Norris, G., Duvall, R., Brown, S., and Bai, S., 2014. EPA positive matrix factorization (PMF) 5.0 fundamentals and user guide, U.S. Environmental Protection Agency, Washington, DC

Paatero, P., and Tapper, U., 1994. Positive matrix factorization: A non-negative factor model with optimal utilization of error estimates of data values, Environmetrics, 5, 111-126, https://doi.org/10.1002/env.3170050203.

Paatero, P., Eberly, S., Brown, S. G., and Norris, G. A., 2014. Methods for estimating uncertainty in factor analytic solutions, Atmospheric Measurement Techniques, 7, 781-797, 10.5194/amt-7-781-2014.

Pata, U. K., 2020. How is COVID-19 affecting environmental pollution in US cities? Evidence from asymmetric Fourier causality test, Air Quality, Atmosphere & Health, 13, 1149-1155, https://doi.org/10.1007/s11869-020-00877-9.

Ren, C., Huang, X., Wang, Z., Sun, P., Chi, X., Ma, Y., Zhou, D., Huang, J., Xie, Y., Gao, J., and Ding, A., 2021. Nonlinear response of nitrate to NOx reduction in China during the COVID-19 pandemic, Atmospheric Environment, 264, 118715, https://doi.org/10.1016/j.atmosenv.2021.118715.

Sharma, S., Zhang, M., Anshika, Gao, J., Zhang, H., and Kota, S. H., 2020. Effect of restricted emissions during COVID-19 on air quality in India, Science of The Total Environment, 728, 138878, https://doi.org/10.1016/j.scitotenv.2020.138878.

Shen, L., Zhao, T., Wang, H., Liu, J., Bai, Y., Kong, S., Zheng, H., Zhu, Y., and Shu, Z., 2021. Importance of meteorology in air pollution events during the city lockdown for COVID-19 in Hubei Province, Central China, Science of The Total Environment, 754, 142227, https://doi.org/10.1016/j.scitotenv.2020.142227.

Shi, Z., Song, C., Liu, B., Lu, G., Xu, J., Van Vu, T., Elliott Robert, J. R., Li, W., Bloss William, J., and Harrison Roy, M., 2021. Abrupt but smaller than expected changes in surface air quality attributable to COVID-19 lockdowns, Science Advances, 7, eabd6696, https://doi.org/10.1126/sciadv.abd6696.

Sulaymon, I. D., Zhang, Y., Hopke, P. K., Hu, J., Zhang, Y., Li, L., Mei, X., Gong, K., Shi, Z., Zhao, B., and Zhao, F., 2021. Persistent high $PM_{2.5}$ pollution driven by unfavorable meteorological conditions during the COVID-19 lockdown period in the Beijing-Tianjin-Hebei region, China, Environmental Research, 198, 111186, https://doi.org/10.1016/j.envres.2021.111186.

Tian, J., Wang, Q., Zhang, Y., Yan, M., Liu, H., Zhang, N., Ran, W., and Cao, J., 2021. Impacts of primary emissions and secondary aerosol formation on air pollution in an urban area of China during the COVID-19 lockdown, Environment International, 150, 106426, https://doi.org/10.1016/j.envint.2021.106426.

Tian, Y., Zhang, Y., Liang, Y., Niu, Z., Xue, Q., and Feng, Y., 2020. $PM_{2.5}$ source apportionment during severe haze episodes in a Chinese megacity based on a 5-month period by using hourly species measurements: Explore how to better conduct PMF during haze episodes, Atmospheric Environment, 224, 117364, https://doi.org/10.1016/j.atmosenv.2020.117364.

Tobías, A., Carnerero, C., Reche, C., Massagué, J., Via, M., Minguillón, M. C., Alastuey, A., and Querol, X., 2020. Changes in air quality during the lockdown in Barcelona (Spain) one month into the SARS-CoV-2 epidemic, Science of The Total Environment, 726, 138540, https://doi.org/10.1016/j.scitotenv.2020.138540.

Wang, H., Ding, J., Xu, J., Wen, J., Han, J., Wang, K., Shi, G., Feng, Y., Ivey, C. E., Wang, Y., Nenes, A., Zhao, Q., and Russell, A. G., 2019. Aerosols in an arid environment: The role of aerosol water content, particulate acidity, precursors, and relative humidity on secondary inorganic aerosols, Science of The Total Environment, 646, 564-572, https://doi.org/10.1016/j.scitotenv.2018.07.321.

Wang, N., Xu, J., Pei, C., Tang, R., Zhou, D., Chen, Y., Li, M., Deng, X., Deng, T., Huang, X., and Ding, A., 2021. Air quality during COVID-19 lockdown in the Yangtze River Delta and the Pearl River Delta: Two different responsive mechanisms to emission reductions in China, Environmental Science & Technology, 55, 5721-5730, https://doi.org/10.1021/acs.est.0c08383.

Wang, Y., Jia, C., Tao, J., Zhang, L., Liang, X., Ma, J., Gao, H., Huang, T., and Zhang, K., 2016. Chemical characterization and source apportionment of $PM_{2.5}$ in a semi-arid and petrochemical-industrialized city,

Northwest China, Science of The Total Environment, 573, 1031-1040, https://doi.org/10.1016/j.scitotenv.2016.08.179.

Wang, Y., Wen, Y., Wang, Y., Zhang, S., Zhang, K. M., Zheng, H., Xing, J., Wu, Y., and Hao, J., 2020. Four-month changes in air quality during and after the COVID-19 lockdown in six megacities in China, Environmental Science & Technology Letters, 7, 802-808, https://doi.org/10.1021/acs.estlett.0c00605.

Wang, Y., Wen, Y., Cui, Y., Guo, L., He, Q., Li, H., and Wang, X., 2022. Substantial changes of chemical composition and sources of fine particles during the period of COVID-19 pandemic in Taiyuan, Northern China, Air Quality, Atmosphere & Health, 15, 47-58, https://doi.org/10.1007/s11869-021-01082-y.

WHO, 2021. WHO global air quality guidelines: Particulate matter ($PM_{2.5}$ and $PM_{10}$), ozone, nitrogen dioxide, sulfur dioxide and carbon monoxide, World Health Organization, Geneva

Xie, Y., Liu, Z., Wen, T., Huang, X., Liu, J., Tang, G., Yang, Y., Li, X., Shen, R., Hu, B., and Wang, Y., 2019. Characteristics of chemical composition and seasonal variations of $PM_{2.5}$ in Shijiazhuang, China: Impact of primary emissions and secondary formation, Science of The Total Environment, 677, 215-229, https://doi.org/10.1016/j.scitotenv.2019.04.300.

Zhang, Q., Zheng, Y., Tong, D., Shao, M., Wang, S., Zhang, Y., Xu, X., Wang, J., He, H., Liu, W., Ding, Y., Lei, Y., Li, J., Wang, Z., Zhang, X., Wang, Y., Cheng, J., Liu, Y., Shi, Q., Yan, L., Geng, G., Hong, C., Li, M., Liu, F., Zheng, B., Cao, J., Ding, A., Gao, J., Fu, Q., Huo, J., Liu, B., Liu, Z., Yang, F., He, K., and Hao, J., 2019. Drivers of improved $PM_{2.5}$ air quality in China from 2013 to 2017, Proceedings of the National Academy of Sciences, 116, 24463, https://doi.org/10.1073/pnas.1907956116.

Zhang, Q., Pan, Y., He, Y., Walters, W. W., Ni, Q., Liu, X., Xu, G., Shao, J., and Jiang, C., 2021. Substantial nitrogen oxides emission reduction from China due to COVID-19 and its impact on surface ozone and aerosol pollution, Science of The Total Environment, 753, 142238, https://doi.org/10.1016/j.scitotenv.2020.142238.

Zhang, R., Sun, X., Shi, A., Huang, Y., Yan, J., Nie, T., Yan, X., and Li, X., 2018. Secondary inorganic aerosols formation during haze episodes at an urban site in Beijing, China, Atmospheric Environment, 177, 275-282, https://doi.org/10.1016/j.atmosenv.2017.12.031.

Zheng, H., Kong, S., Chen, N., Yan, Y., Liu, D., Zhu, B., Xu, K., Cao, W., Ding, Q., Lan, B., Zhang, Z., Zheng, M., Fan, Z., Cheng, Y., Zheng, S., Yao, L., Bai, Y., Zhao, T., and Qi, S., 2020. Significant changes in the chemical compositions and sources of $PM_{2.5}$ in Wuhan since the city lockdown as COVID-19, Science of The Total Environment, 739, 140000, https://doi.org/10.1016/j.scitotenv.2020.140000.

Zhou, H., He, J., Zhao, B., Zhang, L., Fan, Q., Lü, C., Dudagula, Liu, T., and Yuan, Y., 2016. The distribution of $PM_{10}$ and $PM_{2.5}$ carbonaceous aerosol in Baotou, China, Atmospheric Research, 178-179, 102-113, https://doi.org/10.1016/j.atmosres.2016.03.019.

Zhou, H., Lü, C., He, J., Gao, M., Zhao, B., Ren, L., Zhang, L., Fan, Q., Liu, T., He, Z., Dudagula, Zhou, B., Liu, H., and Zhang, Y., 2018. Stoichiometry of water-soluble ions in $PM_{2.5}$: Application in source apportionment for a typical industrial city in semi-arid region, Northwest China, Atmospheric Research, 204, 149-160, https://doi.org/10.1016/j.atmosres.2018.01.017.

Zhou, X., Li, Z., Zhang, T., Wang, F., Tao, Y., Zhang, X., Wang, F., Huang, J., Cheng, T., Jiang, H., Zheng, C., and Liu, F., 2021. Chemical nature and predominant sources of $PM_{10}$ and $PM_{2.5}$ from multiple sites on the Silk Road, Northwest China, Atmospheric Pollution Research, 12, 425-436, https://doi.org/10.1016/j.apr.2020.10.001.

Zíková, N., Wang, Y., Yang, F., Li, X., Tian, M., and Hopke, P. K., 2016. On the source contribution to Beijing $PM_{2.5}$ concentrations, Atmospheric Environment, 134, 84-95, https://doi.org/10.1016/j.atmosenv.2016.03.047.